A CRISPR-Cas9-based system for the dose-dependent study of DNA double strand breaks sensing and repair

Jocelyn Coiffard[1], Olivier Santt[1], Sylvain Kumanski[1],

Benjamin Pardo[2,*] and María Moriel-Carretero[1,*]

[1] *Centre de Recherche en Biologie cellulaire de Montpellier (CRBM), Université de Montpellier – Centre National de la Recherche Scientifique, Montpellier, France*

[2] *Institut de Génétique Humaine (IGH), Université de Montpellier – Centre National de la Recherche Scientifique, Montpellier, France*

* Correspondence to **benjamin.pardo@igh.cnrs.fr** (BP)

maria.moriel@crbm.cnrs.fr (MMC)

Running Title: A CRISPR-Cas9-based tool to study DSBs dose-dependently

Abstract

The integrity of DNA is put at risk by different lesions, among which double strand breaks (DSBs) occur at low frequency, yet remain one of the most life-threatening harms. The study of DSB repair requests tools provoking their accumulation, and include the use of chemical genotoxins, ionizing radiations or the expression of sequence-specific nucleases. While genotoxins and irradiation allow for dose-dependent studies, nucleases expression permits assessments at precise locations. In this work, we have exploited the repetitiveness of the Ty transposon elements in the genome of *Saccharomyces cerevisiae* and the cutting activity of the RNA-guided Cas9 nuclease to create a tool that combines sequence specificity and dose-dependency. In particular, we can achieve the controlled creation of 0, 1, 15 or 59 cuts in cells with an otherwise identical genetic background. We make the first application of this tool to better understand the behavior of the apical kinase of the DNA damage response Tel1. By comparing different strategies to create DNA breaks, we find that Tel1 is capable of forming multiple foci, in striking contrast with other DSB-related proteins. Tel1 foci are in tight contact with the nuclear periphery, therefore suggesting a role for the nuclear membrane in their congregation.

Introduction

Cells are confronted to an enormous amount of spontaneous DNA damage arising from natural sources, such as reactive oxygen, reactive carbonyl and nitrogen species, products of lipid peroxidation or the spontaneous chemical lability of the DNA. In addition, there are external sources of damage such as ionizing radiations, chemicals in food, air and water as well as ultraviolet light. Last, rare exposure as that occurring during chemotherapy and radiotherapy is intentionally aimed at forming damage to the DNA. The lesions resulting from these attacks are of a heterogeneous nature, and can include nucleotide base opening, adducts, crosslinks and single-stranded DNA breaks. DNA double strand breaks (DSBs) can also occur, albeit in lower proportion, yet remaining one of the most life-threatening lesions (1).

This higher deleteriousness is in great part due to the fact that, contrary to single strand breaks, DSBs more frequently lack an appropriate undamaged, complementary strand to

exploit as a repair template. In fact, DSB repair can efficiently occur without such a support through the process of Non-Homologous End Joining (NHEJ) by sealing the broken ends back together (2). This process could be error-prone because short deletions or insertions may occur at junctions, and translocations take place by the joining between two ends from different DSBs (2). Alternatively, if a sequence similar to the broken one exists elsewhere in the genome, it can be used as a template to guide the information retrieval needed to reconstitute the interrupted sequence at the DSB. This process is Homologous Recombination (HR) and, like NHEJ, is not without drawbacks. The homologous sequence needed to support repair may be available in the replicated sister chromatid or in the homologous chromosome. Further, some sequences are repeated and spread throughout the genome. Given that the resolution of the homology copy may end up with an exchange of the neighboring sequences, a process known as crossing-over, only the repair with the sister chromatid warrants a faithful repair (2).

The study of DSB repair requests tools capable of provoking their accumulation. In this sense, genotoxic agents of chemical nature or different types of ionizing radiations are used to damage the genomes of model organisms in a sequence-unspecific manner. A more controlled strategy relies on the expression of proteins whose enzymatic activity creates DSBs at specific DNA target sequences. These can be endonucleases such as restriction enzymes, commonly used *in vitro* for molecular biology (3–8), and meganucleases known to bear a well-defined, rare sequence only present from once to a few times in a given genome (9–13). For example, much of our understanding about DSB repair mechanisms comes from the analysis of HO-mediated DSB in yeast (11). On the one hand, the use of standard restriction enzymes permits the creation of a relatively high number of breaks, at known positions, with ends of a well-defined structure. On the other hand, the use of specific nucleases cutting at single locations allows to focus the study of molecular events with a high degree of precision while ensuring that no break occurring elsewhere influences the outcome of that DSB event. Yet, a limitation of these sequence-targeted tools is that, contrary to the effects obtained when using increasing doses of genotoxins, they cannot be used for dose-dependent studies. In this sense, in a recent elegant study, Gnügge and Symington engineered a battery of strains in which ß-estradiol addition could trigger the expression of one restriction enzyme at a time, each cutting at an increasing number of sites in the genome, ranging from 20 to 96 (14). However, the different *in vivo* enzymatic activities manifested by each enzyme prevent the use of this system for dose-

86 dependent comparative studies. An alternative work exploited the repetitiveness of the
87 transposable Ty elements in *S. cerevisiae* genome to insert 2, 7 or 11 sites that can be cut upon
88 controlled induction of the HO endonuclease (15). Yet, engineering this system was tedious
89 because it implied multiple rounds of cloning, retrotransposition and Southern blot analysis.
90 This system was used to assess molecular events in DSB repair such as resection and
91 checkpoint activation, as monitored by Southern and western blot, respectively (15,16), and
92 the sensitivity of these techniques allowed to assess dose-dependent differences. Yet, if less
93 sensitive techniques important in the field of DSB sensing and repair need to be used, a system
94 with such a restricted number of breaks may not be sufficient.

95 In this work, we have exploited the repetitiveness of the Ty transposon elements in the
96 genome of *S. cerevisiae* and the guide RNA-driven sequence specificity of Cas9 cutting activity.
97 In particular, we have targeted an increasing number of Ty elements by designing specific
98 guide RNAs (gRNAs) that could recognize one or several Ty classes. Upon the controlled
99 induction of Cas9 expression, we can achieve an increasing number of enzymatic cuts (0, 1, 15
100 or 59) *in vivo*. Because Cas9 and the gRNAs are expressed from plasmids, DSBs can be easily
101 induced in cells grown in otherwise identical conditions and with an identical genetic
102 background. Thus, we have generated a tool that overcomes the lack of dose-dependency of
103 expressing restriction enzymes while achieving the maximum number of DSBs in an easily
104 applicable manner, atypical in systems using sequence-specific nucleases.

105 We applied this tool to assess the behavior of the Tel1 apical kinase of the DNA damage
106 response. Contrary to later-acting factors of the DSB repair cascade, fluorescence microscopy
107 is not commonly used to study the very early-acting factors, especially those involved in DSB
108 sensing. Here, we report that Tel1 molecules congregate in the shape of foci in response to
109 diverse sources of DSBs and we dissect how the kinetics of their formation relate to the DSB
110 dose and to the factors acting downstream. Last, we bring the notion that Tel1 can form up to
111 8 foci per cell, in striking contrast with other DSB-related proteins. Tel1 foci distribute as a ring
112 in tight contact with the nuclear periphery, therefore suggesting a role for the nuclear
113 membrane in their congregation.

114

115

116 # Materials and Methods

117 **Reagents** used in this work for cell treatments were zeocin, R25001 ThermoFisher
118 Scientific; camptothecin (CPT), C9911 Sigma-Aldrich; and DAPI, D9542 Sigma-Aldrich.

119

120 **Culture and treatments**: *Saccharomyces cerevisiae* cells carrying plasmids for the
121 expression of the gRNA used to cut the genome and for the expression of the Cas9
122 endonuclease were grown at 25°C in the appropriate selection medium (-uracil, -leucine).
123 Typically, cells were grown in 2 % glucose; prior to the induction of Cas9 expression, cells were
124 shifted to 2 % glycerol and grown overnight at 25°C to ensure complete glucose consumption.
125 When DNA damage was induced using zeocin (100 µg/mL), cells bearing a control plasmid
126 were grown at 25°C in minimal medium with appropriate selection (uracil). Spot assays were
127 carried out in medium selecting the gRNA plasmids (-uracil) and the inducible Cas9
128 expression vector (-tryptophan) containing either 2 % glucose or 2 % galactose as a carbon
129 source. Sensitivity spot assays were carried out using YEPD medium supplemented with
130 either DMSO (control) or with 40 µM CPT. For Nup57 tagging with the red fluorophore
131 tDIMER at its genomic *locus*, the plasmid pRS305-*NUP57*-tDIMER (17) (gift from O. Gadal,
132 Toulouse, France) was linearized with *Bgl*II and transformed into strain MM-144. Pus1 was
133 tagged with mCherry using the plasmid YIplac211-mCherry-*PUS1* (18) (a gift from S.
134 Siniossoglou, Cambridge, UK), which was linearized at the *URA3 locus* with *Bgl*II and inserted
135 by HR in this same *locus* in the strain of interest.

136

137 **Pulsed Field Gel Electrophoresis (PFGE):** Agarose plugs containing
138 chromosomal DNA were made as described (19). Chromosomes were separated at 13°C in a
139 0.9% agarose gel in 0.5× TBE using a Rotaphor apparatus (Biometra) with the following
140 parameters: interval from 100 to 10 s (logarithmic), angle from 120 to 110° (linear), and voltage
141 from 200 to 150 V (logarithmic) during 24 h. The gel was subsequently stained with ethidium
142 bromide for 1 h and washed in water for 30 minutes, then photographed under UV light. For
143 subsequent Southern blot, DNA from gels was transferred to Genescreen Plus membranes

144 (Perkin Elmer). Hybridization was achieved using multiple radioactive probes specific for the
145 chromosome III (*ARS307 locus*) and chromosome IV (*SLX5*, *FOB1*, *RAD9* and *MUS81* genes),
146 and read using a PhosphorImager (Typhoon IP, GE). Three independent biological replicates
147 were performed.

148

149 **Fluorescence Microscopy:** 1 mL of the culture of interest was centrifuged, the
150 supernatant thrown away and the pellet resuspended in the remaining 50 µL. 3 µL of this cell
151 suspension were directly mounted on a microscope slide for immediate imaging of the
152 pertinent fluorophore-tagged protein signals. Imaging was achieved using a Zeiss Axioimager
153 Z2 microscope and visualization, co-localization and analysis done using Image J.

154

155 **Telomere length measurement:** Telomere length was measured by PCR after
156 end labeling with terminal transferase (20,21). End-labeling reactions (40 µL) contained 120 ng
157 genomic DNA, x1 New England Biolabs™ Terminal Transferase Buffer, 1 mM dCTP, 4 units
158 Terminal Transferase (New England Biolabs™) and were carried out at 37°C for 30 minutes
159 followed by heat inactivation at 75°C for 10 minutes. 1/5th volume of 5 M NaCl, 1/80th volume
160 of 1 M $MgCl_2$ and 1 volume of isopropanol were added to the reaction and DNA was
161 precipitated by centrifugation at 17000×g during 15 min. Precipitated DNA was resuspended
162 in 40 µL of ddH_2O. The end-labeled molecules were amplified by PCR using the primer 5′-
163 GCGGATCCGGGGGGGGGGGGGGGG-3′ and 5′-
164 TGTGGTGGTGGGATTAGAGTGGTAG-3′ (X) and 5′-TTAGGGCTATGTAGAAGTGCTG-3′
165 (Y′), respectively. PCR reactions (50 µL) contained between 40 ng and 80 ng of DNA, 1x myTaq
166 buffer, and primers 0.4 µM each. Amplification was carried out with 5 U of MyTaq polymerase
167 (Meridian Biosciences®). The conditions were 95°C, 5 minutes; followed by 35 cycles of 95°C,
168 1 minute; 56°C (Y reaction) / 60°C (X reaction), 20 seconds; 72°C, 5 minutes. Reaction was
169 ended with 5 minutes at 72°C. Samples were visualized in a 2 % agarose gel containing 1×
170 GelRed (Ozyme®).

171

172 **Serial dilution spots assays:** Exponentially growing cells of the indicated
173 genotype were serially diluted 10-fold and 3 µL of each dilution spotted onto the indicated
174 plates, incubated for 3 days at 30°C and photographed.

175 **Analysis of DNA content by flow cytometry:** 430 µL of culture samples
176 at 10^7 cells/mL were fixed with 1 mL of 100% ethanol. Cells were centrifuged for 1 minute at
177 16000 xg and resuspended in 500 µL 50 mM Na-Citrate buffer containing 5 µL of RNase A (10
178 mg/mL, Euromedex, RB0474) and incubated for 2 hours at 50°C. 6 µL of Proteinase K
179 (Euromedex, EU0090-C) were added and after 1 hour at 50°C, cell aggregates were dissociated
180 by sonication (one 3 s-pulse at 50% potency in a Vibracell 72405 Sonicator). 20 µL of this cell
181 suspension were incubated with 200 µL of 50 mM Na-Citrate buffer containing 4 µg/mL
182 Propidium Iodide (FisherScientific). Data were acquired and analyzed on a Novocyte Express
183 (Novocyte).

184

185 **Quantifications, Graphical Representations and Statistical Analyses:** The
186 number of nuclei displaying foci of the analyzed proteins as well as the number of foci present
187 per nucleus were determined visually by the experimenter. Counting was not done in a
188 blinded manner, but three different researchers were implicated in the quantification of
189 experiments to challenge reproducibility. GraphPad Prism was used both to plot the graphs
190 and to statistically analyze the data. The mean value of nuclei displaying foci was calculated
191 for each independent experiment, and the SEM (standard error of the mean) was used to
192 inform on inter-experiment variation. The SEM estimates how far the calculated mean is from
193 the real mean of the sample population, while the SD (standard deviation) informs about the
194 dispersion (variability) of the individual values constituting the population from which the
195 mean was drawn. Given that the goal of our error bars was to describe the uncertainty of the
196 true population mean being represented by the sample mean, we chose to plot the SEM. To
197 plot probability distributions, we converted the actual observations from each category
198 (number of foci) into frequencies by dividing by the total number of observations. To establish
199 the cutting efficiency, band intensities were determined from non-saturated Southern blot

200 images using ImageJ. The signals emanating from cut bands were divided by the addition of
201 signals emanating from both cut and uncut bands, and expressed as a percentage.

202

203 **Strains, plasmids and oligos:** The strains used in this study are presented in
204 Table 1 and were obtained either by classical methods for integration, transformation and
205 crosses, or by CRISPR-Cas9 technology in the case of Tel1 yEGFP-tagging. The plasmids used
206 in this study are presented in Table 2. The relevant sequences for CRISPR-Cas9 manipulations
207 are described in Table 3.

208

209 **Table 1.** Strains used in this study

Simplified Genotype	Full Genotype	Source
WT (W303)	*MAT* a, *ade2, his3, can1, leu2, trp1, ura3*, GAL+, psi+, *RAD5*$^{+}$	PP870, Philippe Pasero
tel1Δ	*MAT* a, *ura3-52, leu2-3,112, his3-i200, trp1-1, trp1-1, lys2-801, tel1ΔKAN*^{R}	PP1217, Philippe Pasero
Rad52-YFP Rfa1-CFP mCherry-Pus1	*MAT* a, *ade2, his3, can1, leu2, trp1, ura3, RAD52-YFP RFA1-CFP mCherry-PUS1::URA3*	PP3558, Philippe Pasero
yEGFP-Tel1 mCherry-Pus1	*MAT* a, *ade2, his3, can1, leu2, trp1, ura3*, GAL+, psi+, *RAD5*$^{+}$, *yEGFP-TEL1, mCherry-PUS1::URA3*	MM-40, this study
yEGFP-Tel1	*MAT* a, *ade2, his3, can1, leu2, trp1, ura3*, GAL+, psi+, *RAD5*$^{+}$, *yEGFP-TEL1*	MM-144, this study
yEGFP-Tel1 Nup57-tDimer	*MAT* a, *ade2, his3, leu2, trp1, ura3, yEGFP-TEL1 Nup57-tDIMER-RFP::LEU2*	MM-282, this study

210

211 **Table 2.** Plasmids used in this study

Simplified Name	Detailed Information	Source
pEmpty	pRS316	Benjamin Pardo
pMEL10	pMEL10	(22) Addgene #107916
p-*gRNA(x 1 cut)*	pMEL10-gRNA(Ty5)	This study
p-*gRNA(x 15 cuts)*	pMEL10-gRNA(Ty2)	This study
p-*gRNA(x 59 cuts)*	pMEL10-gRNA(Ty2 + Ty1)	This study
p*GALp-CAS9*	pRS415-*GALp-CAS9-CYC1t*	(23) Addgene #43804
p-gRNA(*TEL1p*)	pMEL14-gRNA(*TEL1p*)	This study

p-*TEF1p-CAS9*	pRS414-*TEF1p-CAS9-CYC1t*	(23) Addgene #43802
p-yEGFP	pKT128	(24)
p*NUP57*-tDIMER	pRS305-*NUP57*-tDimerRFP	(17)
p-mCherry-*PUS1*	YIplac211-mCherry-*PUS1*	(18)

212

213 **Table 3.** Relevant sequences used in this study (PAM is underlined)

Simplified name	Sequence	Goal
Ty5 (x 1 cut)	TGTGCAATCACCTGATGATGTGG	Target of gRNA(x 1-cut)
Ty2 *(x 15 cuts)*	GACATTCCTATAAATGCCATTGG	Target of gRNA(x 15-cuts)
Ty2 & Ty1*(x 59 cuts)*	ATAAGACCTCCACCACATTTAGG	Target of gRNA(x 59-cuts)
TEL1 promoter	AATCAGTGTAACATAGACGATGG	Target of gRNA(*TEL1*p)
DSBR-Tel1p-fw	CAGGAAATTCGAAAAAAAAGCCTTCAAAGAAAAGGGAAATCAGTGTAACATAGACGatgtctaaaggtgaagaattattc	PCR of the repair product to build yEGFP-Tel1
DSBR-Tel1p-rv	ATAGAAAGTTTAAAGTTTCTACAATCCCATGATCCTCCATtaaaccagcaccgtcacctttgtacaattcatccataccatg	PCR of the repair product to build yEGFP-Tel1

214

215 # Results

216 **A genetic system to create DNA double strand breaks in an inducible and dose-dependent**
217 **manner**

218 In order to generate multiple DSBs, we targeted repeated DNA by using the CRISPR-
219 Cas9 technology (25). Among the most abundant classes of repeats in *S. cerevisiae* are
220 retrotransposons (Ty elements), which represent about 3% of the genome (26), and whose
221 targetability by the CRISPR-Cas9 technology has already been demonstrated in a study aimed
222 at engineering translocations in a controlled manner (27). Based on the sequenced genome of
223 the W303 yeast strain (28), we designed guide RNAs (gRNAs) to target the sole complete Ty5
224 element (1 cut), the 15 copies of Ty2 (15 cuts) and both the closely related Ty1 and Ty2 (59 cuts)
225 (Fig 1A). The sequences for the gRNAs were cloned in multicopy expression plasmids,
226 different from the one expressing the Cas9 nuclease under the control of the galactose-
227 inducible GalL promoter (22,23).

228 To assess the performance of the system, we initially tested viability upon inducing
229 Cas9 expression in cells simultaneously expressing no guide RNA (gRNA) and thus no DSB

230 (x 0), or the gRNAs cutting the genome once (x 1), 15 times (x 15) or 59 times (x 59), respectively.
231 By spotting serial dilutions of such cells in medium containing glucose (no Cas9 expression)
232 or galactose (Cas9 expression), we observed that cells simultaneously expressing Cas9 and any
233 gRNA, thus suffering from constant DNA cutting, had difficulties for (x 1 cut) or were
234 incapable of (several cuts) proliferating (Fig 1B, galactose). This genetic evidence suggests that
235 the system is functional.
236

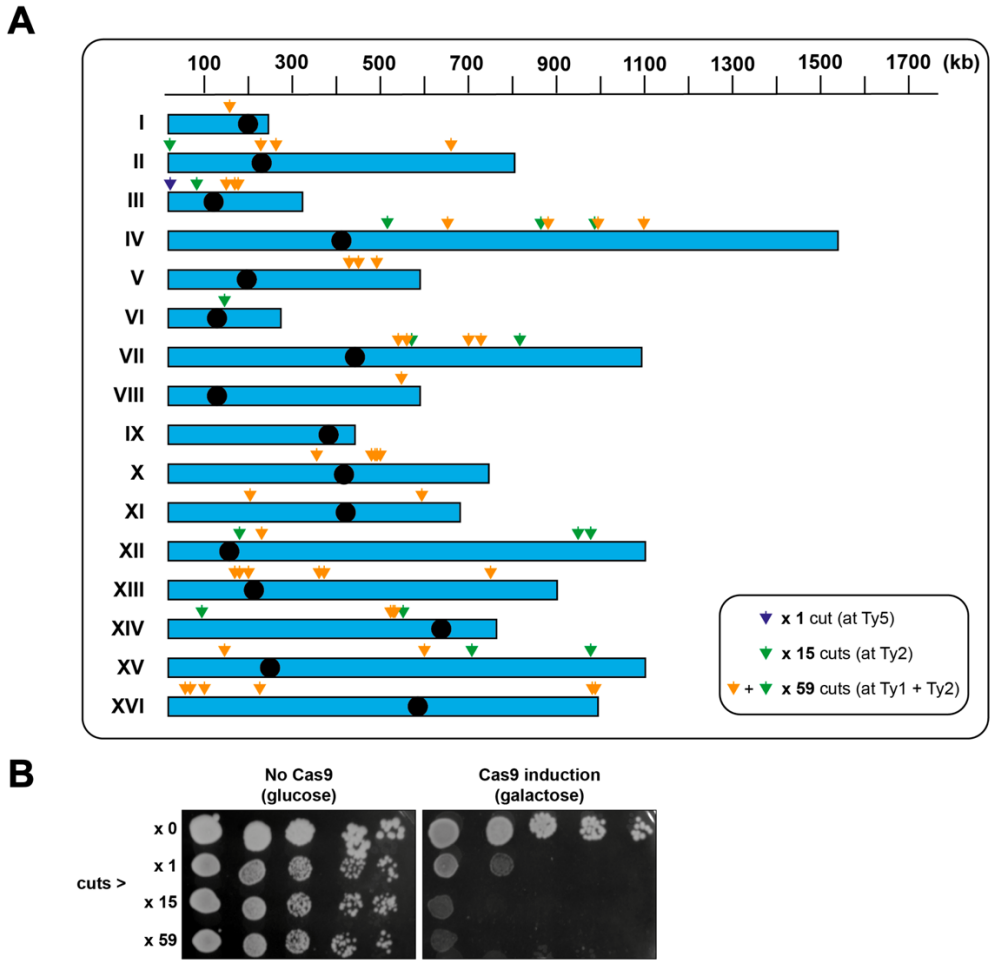

237

238 **Fig 1. Design of the CRISPR-Cas9-based system to induce DSBs in a dose-dependent**
239 **manner**

240 **A.** Scheme of the sixteen *S. cerevisiae* chromosomes (blue boxes), in which the black circles
241 mark the relative position of the centromeres. Color-coded arrows mark the approximate Ty
242 positions targeted by the designed gRNAs. In more detail, the x 1-cut gRNA targets the single
243 Ty5 (dark blue arrow), the x 15-cuts gRNA targets the Ty2 sites (green arrows), and the x 59-
244 cuts gRNA targets both Ty2 and Ty1 sites (orange and green arrows).

245 **B.** *S. cerevisiae* WT cells were transformed with the vector bearing an inducible Cas9 and with
246 the vector expressing the relevant gRNA to achieve the desired number of cuts. 10-fold serial
247 dilutions of cells exponentially growing in glucose to prevent Cas9 expression were spotted
248 onto selective minimal medium plates supplemented with the following carbon source: either
249 glucose, to monitor the loading control; or galactose, to induce Cas9 expression.
250
251 We next wanted to provide a physical and more quantitative characterization of the
252 system. To this end, we grew cells overnight until they reached exponential phase in medium
253 selective for the Cas9 and gRNAs plasmids and with glycerol as the carbon source, allowing a
254 robust and controlled induction of Cas9 upon galactose addition. Cells were recovered and
255 processed for flow cytometry and Pulsed Field Gel Electrophoresis (PFGE) analyses before
256 induction of Cas9 expression and every 2 hours thereafter during 8 hours. The analysis of DNA
257 contents by flow cytometry showed a mild but progressive accumulation of cells in G_2/M in
258 the x 15-cuts and x 59-cuts systems (Fig 2A, red asterisks). These results are consistent with the
259 activation of the DNA damage checkpoint, which halts the cell cycle progression in G_2/M in
260 response to DSBs (29).
261 Separation of chromosomes by PFGE allows for the detection of broken DNA
262 molecules. No broken DNA molecules could be detected at any of the time-points of the x 0-
263 cut kinetics. However, modest smeared signals were visible in the ethidium bromide-stained
264 gels at late times of the x 15-cuts and x 59-cuts gRNA kinetics (Fig 2B and S1 Fig). Yet, the
265 strongest evidence of molecules being broken emanated from the latest time-points in the x
266 59-cuts system, when signals corresponding to full chromosomes started to fade away.
267 To provide formal proof of the breaks, the DNA was transferred and membranes
268 subjected to Southern blot using either a probe directed to the chromosome III or a mix of four
269 probes directed against various locations on chromosome IV. As a result, a time- and dose-
270 dependent pattern of chromosome fragments could be observed (Fig 2C), confirming the
271 proficiency of the system.
272

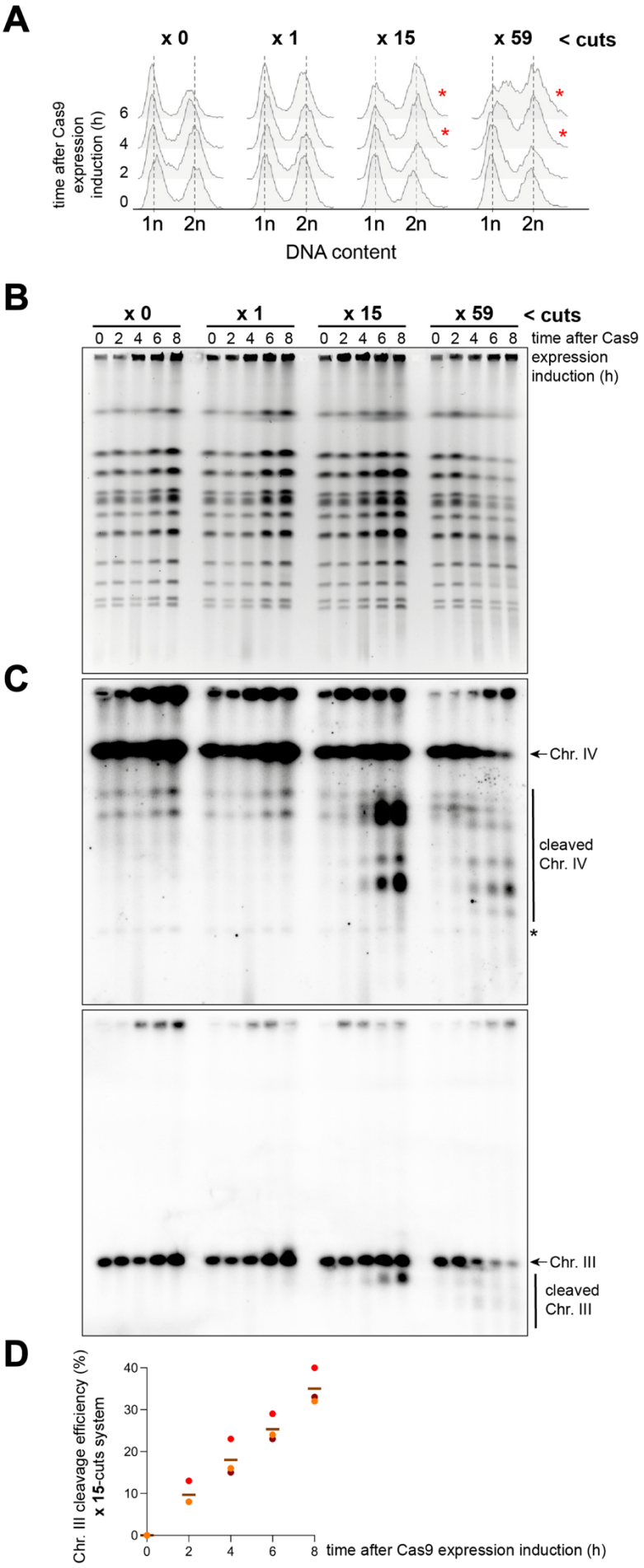
A
x 0
x 1
x 15
x 59
< cuts
time after Cas9 expression induction (h)
6
4
2
0
1n 2n
DNA content
B
x 0
x 1
x 15
x 59
< cuts
0 2 4 6 8
time after Cas9 expression induction (h)
C
Chr. IV
cleaved Chr. IV
Chr. III
cleaved Chr. III
D
Chr. III cleavage efficiency (%) x 15-cuts system
40
30
20
10
0
0 2 4 6 8
time after Cas9 expression induction (h)

273

274 **Fig 2. Physical characterization of the DSB-inducible system**

275 **A.** *S. cerevisiae* WT cells were transformed as in Fig 1B, and a culture of cells growing
276 exponentially in selective minimal medium with glycerol as the carbon source was prepared.
277 A sample was taken at time 0 (before induction). After the addition of galactose, samples were
278 taken at the indicated time points to assess cytometry profiles. n and 2n refer to the DNA
279 content, thus serving as an estimate of the number of cells in G_1 and G_2 phases of the cell cycle,
280 respectively. The red asterisks indicate the time-points at which an increase in the number of
281 cells in G_2/M is detected when compared to the no-cut condition.

282 **B.** *S. cerevisiae* WT cells were transformed as in Fig 1B, and a culture of cells growing
283 exponentially in selective minimal medium with glycerol as the carbon source was prepared.
284 A sample was taken at time 0 (before induction). After the addition of galactose, samples were
285 taken at the indicated time points. Cells were processed for Pulsed Field Gel Electrophoresis
286 (PFGE). This technique allows for the separation of chromosomes. The PFGE gel was dyed
287 with ethidium bromide.

288 **C.** Southern blot against the DNA from the PFGE shown in **(B)** using one probe targeting
289 chromosome III and four probes targeting chromosome IV. Bands corresponding to full-length
290 chromosomes III and IV are indicated. The asterisk indicates a remaining band corresponding
291 to chromosome III after incomplete stripping of the radioactive probe from the membrane.

292 **D.** Quantification of chromosome III cleavage efficiency after Cas9 induction in the x 15-cuts
293 system. The mean values (brown bar) and the individual values (circles) from three
294 independent experiments (indicated by different colours) are plotted for each time point of the
295 time course experiment shown in **(C)**.

296

297 We subsequently performed a deep restriction analysis of chromosome cleavage by
298 Cas9 in order to verify the specific cleavages in Ty elements indicated in Fig 1A. We used the
299 known sizes of the full-length chromosome bands from the ethidium bromide-stained gel to
300 infer the sizes of the chromosome fragments that appeared 8h after Cas9 induction on the
301 Southern blot membrane (S1 Fig). In the x 15-cuts system, the chromosome III is expected to
302 be cleaved once, generating a ~254 kb fragment, which we could detect by using a probe
303 targeting this fragment (Fig 3A). We took advantage of this unique cleavage to quantify the
304 cleavage efficiency, which increased progressively to reach a mean value of 35% 8 h after Cas9

induction (Fig 2D). In this same system, 3 cuts are expected in chromosome IV. These cuts can generate various fragments corresponding to the complete or partial cleavage of the chromosome IV (Fig 3A).

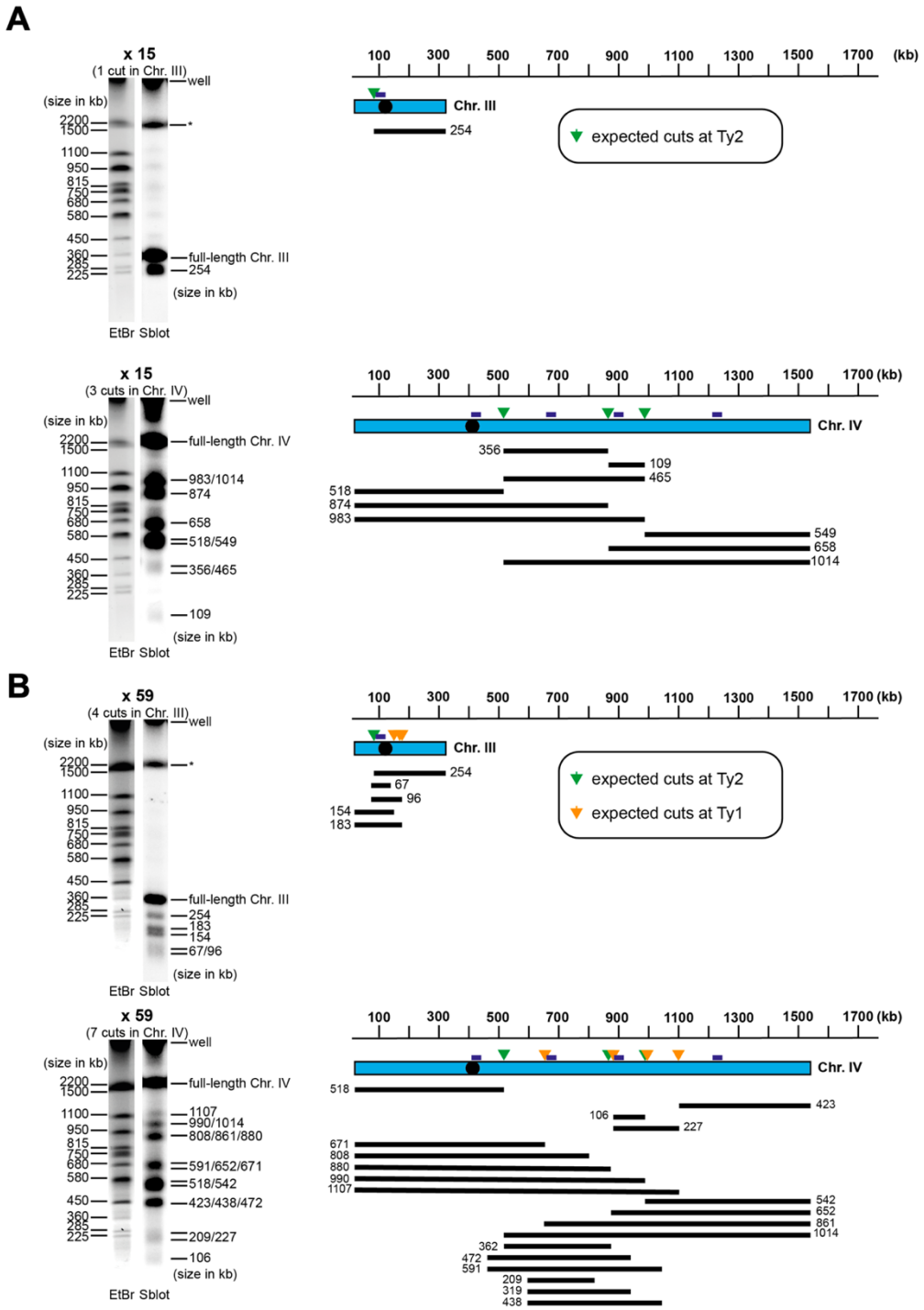

Fig 3. Restriction analyses of chromosome cleavage

311 **A, B.** Restriction analysis of chromosomes III and IV cleaved by Cas9 in the x 15-cuts **(A)** and
312 x 59-cuts **(B)** systems. Full-length chromosome sizes (from ethidium bromide-stained gel;
313 EtBr) and inferred fragment sizes (from Southern Blot; Sblot) are indicated in kb. The asterisk
314 indicates a remaining band corresponding to chromosome IV after incomplete stripping of the
315 radioactive probe from the membrane. The approximate Ty positions targeted by the designed
316 gRNAs and the probes used for Southern blot analysis are indicated on chromosome schemes.
317 Restriction patterns are depicted, with expected chromosome fragments sizes, out of both full
318 and partial digestions, indicated in kb. Shown images come from the experiment shown in S1
319 Fig.
320
321 The Southern blot analysis revealed the presence of bands corresponding to all the
322 expected sizes of the chromosome fragments (Fig 3A). We performed the same analysis for the
323 x 59-cuts system, in which four cuts in chromosome III and seven cuts in chromosome IV are
324 expected. We could identify chromosome fragment bands corresponding to all expected
325 restriction patterns thanks to various probes targeting the regions between the cleavage sites
326 (Fig 3B). Overall, we conclude that, albeit with a modest cutting efficiency, our CRISPR-Cas9-
327 based system creates site-specific DSBs in a dose-dependent manner.
328
329 **The Cas9-induced DSBs system allows monitoring the dose-dependent kinetics of DNA**
330 **repair by microscopy**
331 We exported the system (Cas9 and gRNAs plasmids) to an otherwise WT strain in
332 which early actors of the HR DNA repair pathway were fluorescently tagged. In more detail,
333 the Rfa1 component of the heterotrimeric RPA complex, in charge of binding exposed single
334 stranded DNA (ssDNA), was tagged with CFP at its C-terminus; Rad52, which substitutes
335 RPA for Rad51 on ssDNA to initiate homology search, was tagged with YFP at its C-terminus;
336 and the nucleosoluble protein Pus1 was tagged with mCherry at its N-terminus to clearly
337 define the nucleus. As above, cells were grown overnight to mid-log phase in selective
338 medium plus glycerol, then galactose was added to initiate Cas9 expression. Cells were
339 visualized with the help of a fluorescence microscope and images acquired before Cas9
340 expression induction and every hour during 7 hours thereafter. We counted the percentage of
341 nuclei in the population displaying Rfa1-CFP and Rad52-YFP foci (at least one focus). The

342 percentage of nuclei basally displaying Rfa1 foci was of 10 % and fluctuated around this value
343 for each time point when Cas9 was expressed in the absence of any gRNA (Fig 4A,B,D, x 0).
344 Likewise, the lack of DSB maintained a basal level of 4 % of the nuclei displaying Rad52-YFP
345 foci (Fig 4A,C,E, x 0). These data agree with previously reported basal levels for these factors
346 (30), and further confirm that, in the absence of any gRNA, Cas9 alone does not trigger any
347 accumulation of DNA damage. Importantly, the expression of gRNAs driving an increasing
348 number of DSBs permitted us to draw the following observations: First, the system seems to
349 be slightly leaky for, in the absence of Cas9 expression induction, the basal number of Rfa1
350 and Rad52 foci-forming cells correlatively increased in cells expressing the gRNAs leading to
351 more DSBs (Fig 4B,C). Second, this confirmed the proficiency of the system, since the initial
352 percentage of foci-displaying cells increased with time when the x 1-, x 15- and x 59-cuts
353 gRNAs were present in the cells (Fig 4D,E). Third, the proportion of nuclei displaying Rfa1
354 foci was consistently double than that of nuclei bearing Rad52 foci, probably reflecting the
355 increased residence time of resected filaments in comparison with the process of homology
356 search (Fig 4C,D). Fourth, and as a general rule, gRNAs driving a higher number of DSBs led
357 to an increased number of cells bearing Rfa1 and Rad52 foci (*i.e.* x15 > x1 > x0), with the higher
358 mean values being of 45% of cells bearing Rfa1 foci and 27% showing Rad52 foci (Fig 4D,E).
359 Surprisingly, from 5 hours onwards, creating 15 DSBs in the genome triggered more Rfa1 foci
360 accumulation than inducing 59 DSBs, and a much faster (although equal in value)
361 accumulation of Rad52 foci (Fig 4D,E, and see discussion). Finally, we observed that increasing
362 numbers of DSBs also increased the number of individual Rfa1 foci per nucleus (S2 Fig). This
363 was not the case for Rad52 foci, which were previously described to be repair centers capable
364 of recruiting more than one DSB (31). Overall, these results suggest that the *bona-fide* DSBs
365 created by our system can be monitored by fluorescence microscopy thus providing insights
366 into the kinetics of DNA repair.
367

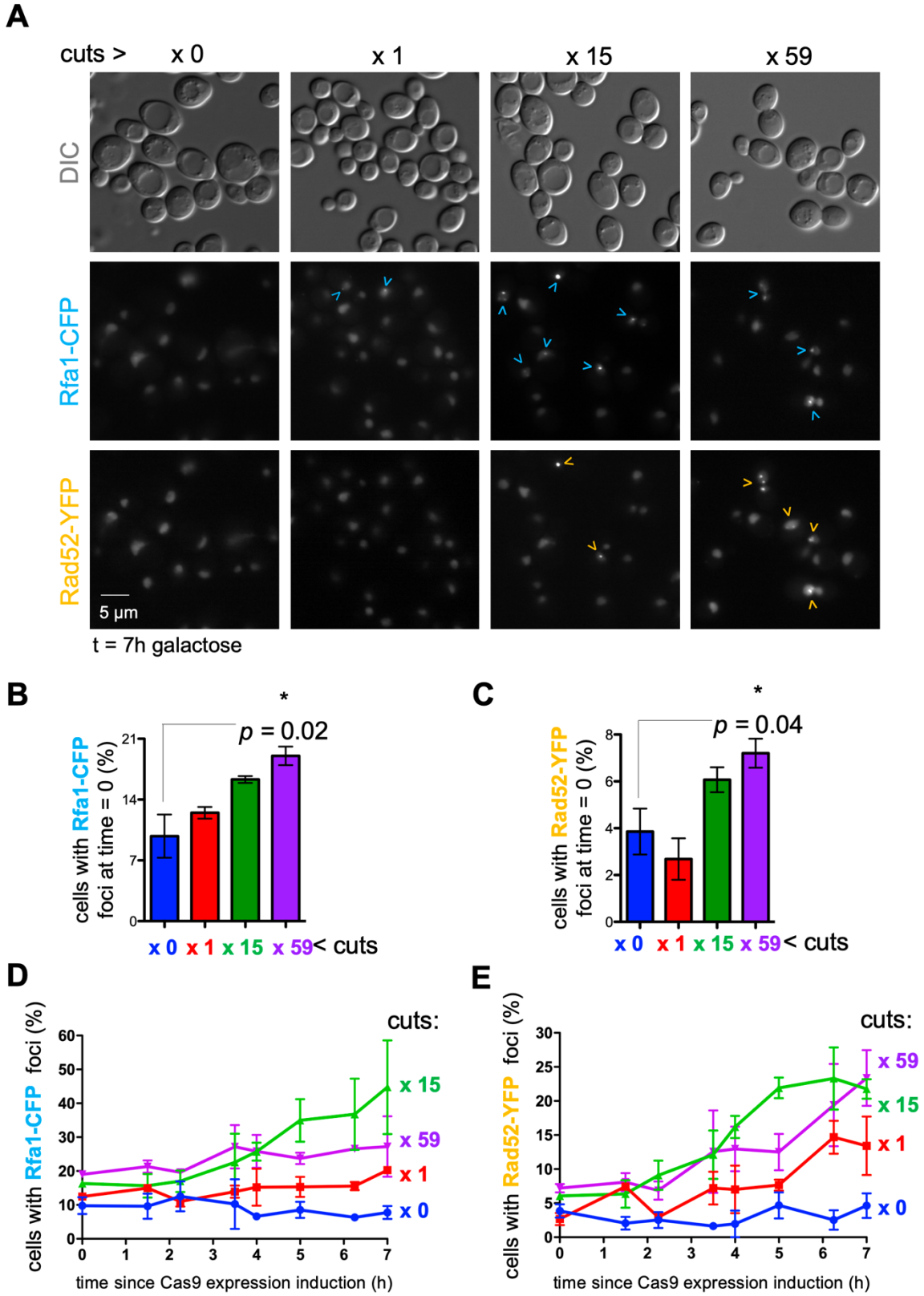

Fig 4. Characterization of DNA repair foci formation in response to increasing Cas9-driven cuts

A. WT cells transformed with the vector expressing an inducible Cas9 and the plasmid expressing the gRNA driving the desired number of cuts grown to exponential phase in

373 selective minimal medium using glycerol as the carbon source. A sample was taken at time 0
374 before galactose was added to induce Cas9 expression, samples retrieved at the indicated
375 times, and cells inspected by microscopy. Representative images of Differential Interference
376 Contrast (DIC), Rfa1-CFP and Rad52-YFP channels are shown. Arrowheads point at foci
377 formed by the fluorescently tagged proteins.
378 **B.** Percentage of cells in the population displaying at least one focus of Rfa1-CFP in samples
379 from (A) at time 0 (no galactose addition). The bar height is the mean of three independent
380 experiments, and the error bars represent the SEM out of those three experiments. At least 150
381 cells were considered per condition, time and experiment. The * and the *p*-value indicate the
382 significance of the difference of the means after applying a *t*-test. Each cut scenario is
383 associated with one colour, and this code is maintained in subsequent sections.
384 **C.** Percentage of cells in the population displaying at least one focus of Rad52-YFP in samples
385 from **(A)** at time 0 (no galactose addition). Details as in **(B)**.
386 **D.** Percentage of cells in the population displaying at least one focus of Rfa1-CFP in samples
387 from **(A)** at different times since galactose addition. Each point is the mean of three
388 independent experiments, and the error bars represent the SEM out of those three experiments.
389 **E.** Graph showing the percentage of cells in the population displaying at least one focus of
390 Rad52-YFP in samples from **(A)** at different times after galactose addition. Details as in **(D)**.
391
392 **Exploiting the dose-dependent DSB system to study Tel1 foci**
393 Fluorophore-tagging of multiple proteins has allowed the establishment of the
394 temporal kinetics from DSB sensing till late steps of its repair (30,32). Yet, compared to the
395 number of works assessing the formation, persistence, dissolution or frequency of foci of DNA
396 repair proteins such as Rad52, the study of very early acting factors such as DSB sensors is
397 under-assessed. DSBs sensing is orchestrated by the early arrival of the MRX (MRN in
398 humans) complex and its immediate binding by the apical kinase of the DNA Damage
399 Response Tel1 (ATM in humans). These foci can form at any stage of the cell cycle, persist if
400 resection is not implemented, as in *SAE2* deletion mutants (30,33) and, in agreement with their
401 early role, do not depend on the ssDNA-coating complex RPA (30). Still, in contrast to Mre11
402 foci, which have attracted more interest (16,33), Tel1 study by microscopy has been assessed
403 in only one study (30). This little interest may relate to the fact that the absence of Tel1 hardly

404 sensitizes cells to genotoxic agents, with the exception of Topoisomerase I trapping by
405 camptothecin (CPT) (34), presumably because its deficiency is often compensated by the other
406 apical kinase Mec1 (35,36). Yet, accurate sensing, proper processing and timely checkpoint
407 activation upon DSBs depend on Tel1, and therefore the alternative orchestration by Mec1 may
408 not reflect the physiological pathway that the lesions should have triggered. Moreover, in the
409 event of an increasing number of simultaneous DSBs, Tel1 signaling becomes critical in the
410 absence of Mec1 (16).

411 We have tagged Tel1 with yeast-enhanced-GFP (yEGFP) at its N-terminus, a location
412 reported to preserve its function (30,37), while conserving its natural promoter. In agreement,
413 strains bearing this modification were as proficient as their isogenic WT in tolerating CPT, as
414 assayed by serial dilution spotting, and in contrast to *tel1Δ* cells (Panel A in S3 Fig). Other than
415 in DSB signaling, Tel1 is key in preserving telomere length, which can be measured by sub-
416 jecting samples to terminal transferase treatment followed by PCR-driven telomere amplifica-
417 tion (20,21). We have monitored both X and Y' telomere length and observed similar sizes in
418 WT and in derived yEGFP-Tel1 cells, in marked contrast with the shorter products observed
419 for *tel1Δ* cells (Panel B in S3 Fig). Thus, we conclude that the fluorescent tag at the N-terminus
420 of Tel1 does not alter its biology and can be used to assess functional questions.

421 Inducing DSBs with the CRISPR-Cas9 dose-dependent system led to Tel1 forming
422 subnuclear foci (Fig 5A) whose morphology and size did not differ from those reported after
423 DSBs induction with ionizing radiations (30), or other DNA damage-related foci, for example
424 of Rad52 or Rfa1 (Fig 4). Of note, we always observed these foci in the periphery of the nucleus
425 (Fig 5A). Second, the basal level of cells presenting Tel1 foci in the population was low, at
426 around 4% (Fig 5A), suggesting that the basal localization of Tel1 at telomeres does not lead to
427 foci formation. Third, the progressive accumulation of DSBs, dependent on time and on gRNA
428 type, matched a parallel increase in the percentage of cells in the population displaying Tel1
429 foci (Fig 5A, x 0 < x 1 < x 15 < x 59). In this sense, the maximum obtained value, of 20 % (x 59
430 cuts at 7 h), was in striking concordance with the percentage of cells displaying Rad52 foci in
431 the same condition (Fig 4E). The concordance was also manifested as a transient advantage in
432 accumulating the foci when 15 DSBs were induced (Fig 5A, x15 at 3h). Concerning the number
433 of Tel1 puncta per nucleus, even after 7 hours of induction of the maximum number of cuts,
434 positive cells rarely displayed more than 1 Tel1 focus (Panel C in S3 Fig). Thus, the N-terminal

435 tagging of Tel1 by yEGFP represents a performant tool allowing sensitive studies by
436 microscopy approaches.
437

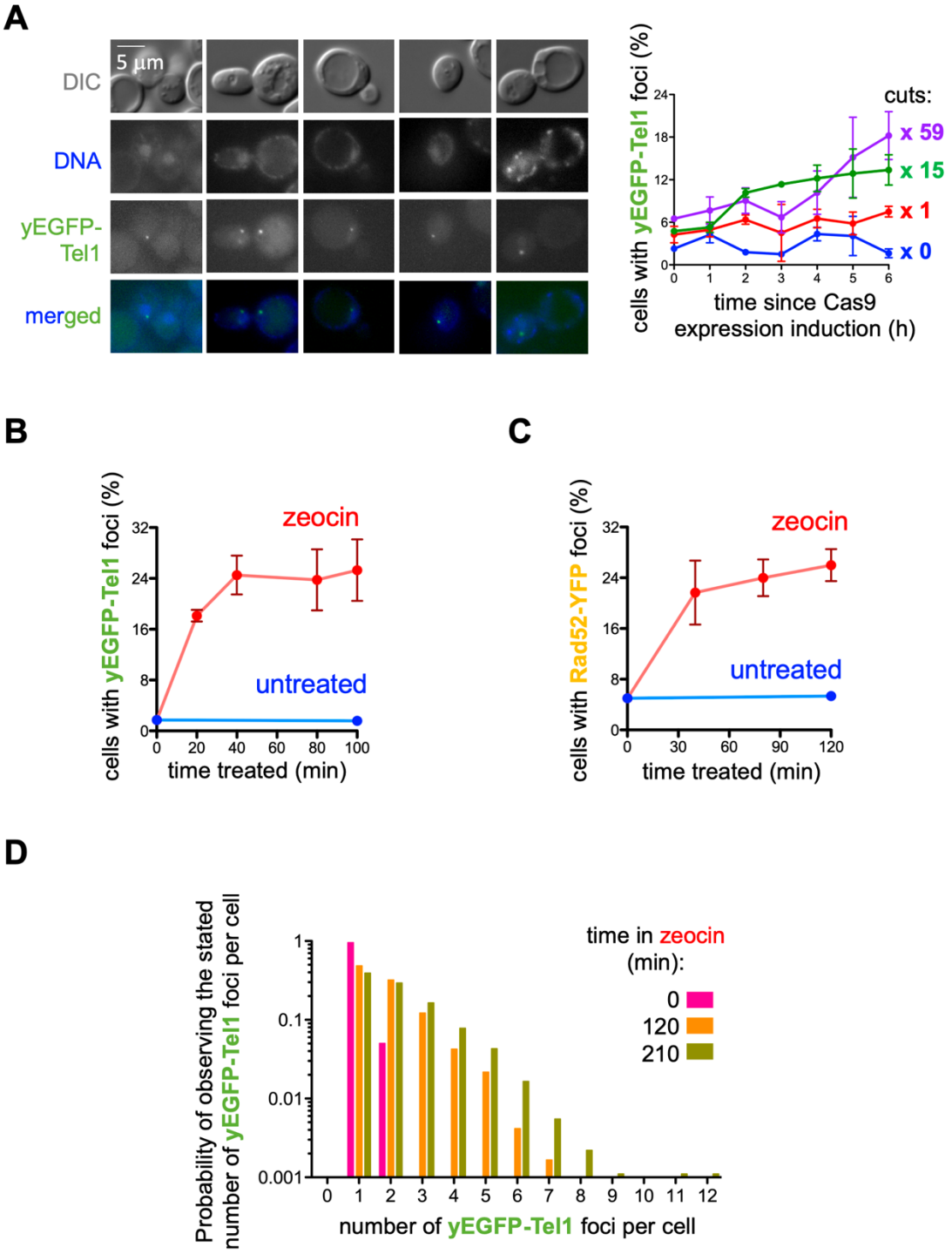

438
439 **Fig 5. Characterization by microscopy of Tel1 behavior in response to DSBs**
440 **A.** yEGFP-Tel1 cells transformed with the vector expressing an inducible Cas9 and the plasmid
441 expressing the gRNA driving the desired number of cuts grown to the exponential phase in

442 selective minimal medium using glycerol as the carbon source. Samples were taken at time 0
443 before galactose was added to induce Cas9 expression, and retrieved at the indicated times
444 after induction, and cells inspected by microscopy in search of Tel1 foci. Representative images
445 are shown on the left, for which DNA (both nuclear and mitochondrial) can be visualized with
446 DAPI. The graph on the right shows the percentage of cells in the population displaying at
447 least one focus of yEGFP-Tel1 at different times since galactose addition. Each point is the
448 mean of three independent experiments, and the error bars represent the SEM out of those
449 three experiments. At least 150 cells were considered per time, condition and experiment.
450 **B.** An otherwise WT strain tagged with yEGFP at the N-terminus of Tel1 and with mCherry at
451 the N-terminus of Pus1 was transformed with an empty vector allowing its growth in minimal
452 selective medium. Cells were exposed to 100 µg/mL zeocin and samples retrieved for analysis
453 by fluorescence microscopy at the indicated times. The graph shows the percentage of cells in
454 the population displaying at least one focus of yEGFP-Tel1 at different times. Each point is the
455 mean of three independent experiments, and the error bars represent the SEM out of those
456 three experiments. At least 150 cells were considered per time, condition and experiment.
457 **C.** Details as in (B) but to score the formation of Rad52-YFP foci.
458 **D.** The foci count data obtained from the cells harbouring at least one focus presented in the
459 three experiments described in **(B)** were exploited to build a probability frequency
460 distribution. In brief, the number of Tel1 foci per nucleus was counted and a frequency
461 histogram was drawn. Since the three independent experiments provided similar profiles, all
462 the values were merged to build a more robust distribution. The graph illustrates the
463 probability of finding a nucleus with a given number of Tel1 foci for cells not being exposed
464 to zeocin, or exposed for 120 or for 210 minutes (pink, orange and green bars, respectively).
465

466 **Tel1 forms foci at the nuclear membrane upon genotoxin-induced DSBs**

467 Genotoxins are regularly used to create DNA lesions, among which DSBs. For example,
468 zeocin is reported to trigger the accumulation of DSBs, but also ssDNA breaks (38). Moreover,
469 given the chemical nature of their action, break ends created this way may be heterogeneous,
470 or "dirty". To learn further, we wanted to compare whether chemical induction of DSBs
471 recapitulated Tel1 foci formation upon the induction of DSBs by Cas9. We grew cells in the
472 same conditions as for the Cas9-DSB-inducing system experiments. We acquired images of

473 these untreated cells and then at intervals till 100 min of exposure to 100 μg/mL zeocin. We
474 could observe that Tel1 foci formed at the same frequency in the population as when DSBs
475 were induced by Cas9 (Fig 5B). In more detail, a maximum value of 24 % was reached at 40
476 min that was invariably maintained till 100 min, and monitoring the percentage of cells bearing
477 Rad52-YFP foci demonstrated a strikingly similar kinetics (Fig 5C). Yet, a remarkable
478 difference between Cas9- and zeocin-induced cuts related to the number of Tel1 foci per cell.
479 In fact, we observed that the probability of finding positive cells with more than one (up to 8)
480 Tel1 focus per nucleus increased as time passed by under zeocin treatment (Fig 5D).
481 Interestingly, these Tel1 foci distributed in the shape of a ring, which regularly sat as "a crown
482 on top" of the nucleus (Fig 6A). As such, their subnuclear localization seemed to be mostly
483 peripheral. To consolidate the observation that Tel1 seemed to form in tight proximity to the
484 nuclear envelope, we simultaneously monitored Tel1 foci and the nucleoporin Nup57 marked
485 in its C-terminus with a tDIMER-RFP moiety. In support, Tel1 foci were neatly and recurrently
486 found close to Nup57-tDIMER signals (Fig 6B), with a maximum distance between the
487 maximal intensities of both adjacent signals of 0.3 μm (Fig 6B, right).
488 Overall, we conclude that yEGFP-Tel1 represents an important tool to accurately
489 monitor the very early stages of DSBs signaling, irrespective of whether they are enzymatically
490 or chemically induced. Furthermore, while at the population level the formation of Tel1 foci is
491 perfectly mirrored by the pre-existing tool Rad52-YFP, the subnuclear distribution and
492 congregation patterns of Tel1 foci are different, suggesting the existence of yet unknown
493 aspects of DSBs initial processing.
494

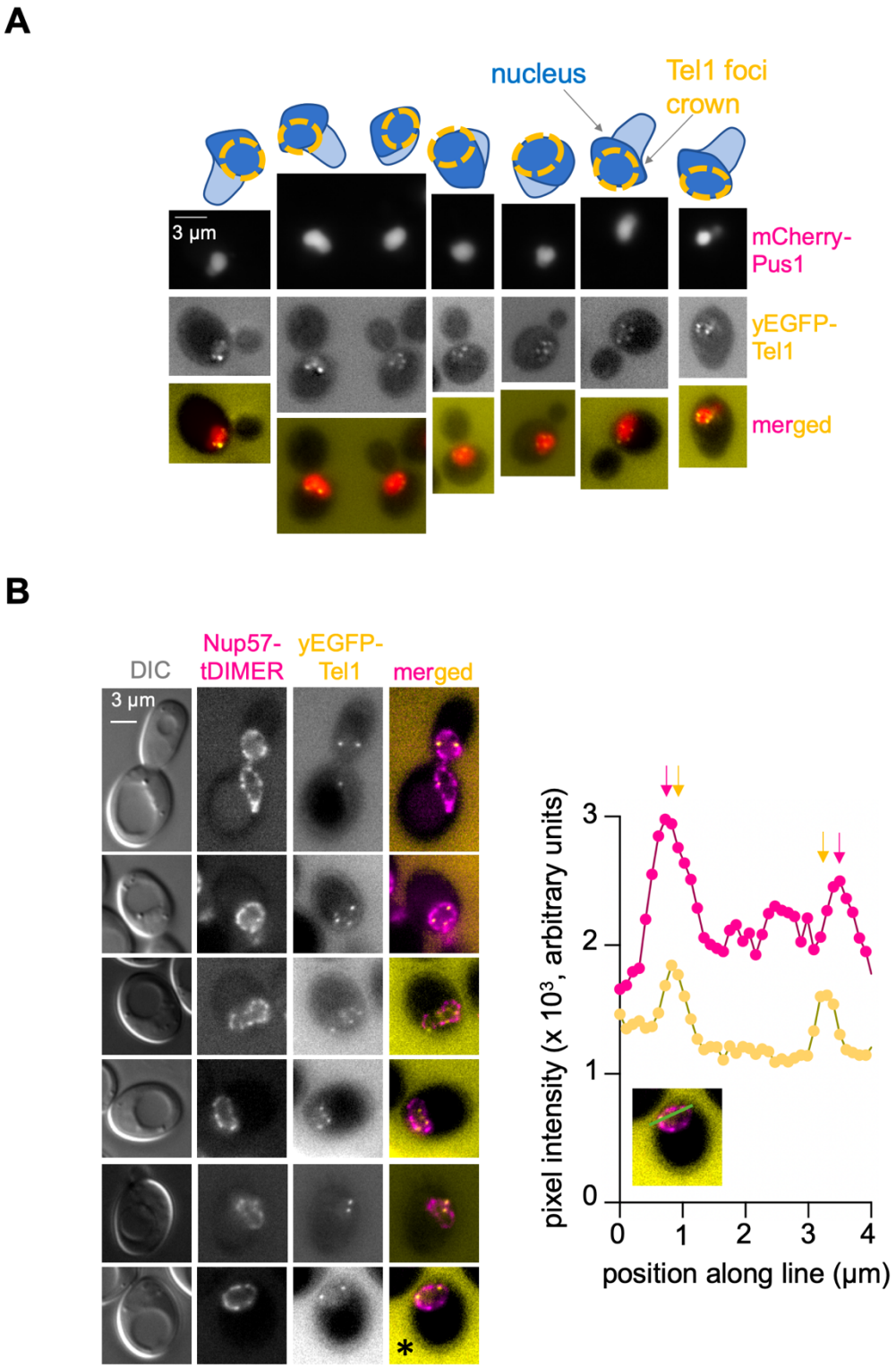

Fig 6. Characterization of the proximity of Tel1 foci to the nuclear membrane

A. An otherwise WT strain was tagged with yEGFP at the N-terminus of Tel1 and with mCherry at the N-terminus of the nucleosoluble protein Pus1 in order to define the nucleoplasm. The subcellular localization of Tel1 was assessed by fluorescence microscopy in response to 100 µg/mL zeocin. Images of both channels as well as their merging are shown.

501 Since Pus1 signals are slightly less intense in some nuclear regions, notably the nucleolus, this
502 difference is represented by using two different tonalities of blue. Schematic drawings of each
503 imaged nucleus mimic the arrangement of the observed structures to facilitate visualization.
504 **B. Left:** An otherwise WT strain was tagged with yEGFP at the N-terminus of Tel1, and with
505 tDIMER-RFP at the C-terminus of the nucleoporin Nup57 with the goal of defining the nuclear
506 periphery. The relative position of Tel1 foci with respect to nucleoporin signals was assessed
507 by fluorescence microscopy after exposing the cells for 2 h to 100 μg/mL zeocin. Images of the
508 Differential Interference Contrast (DIC), RFP and GFP channels, as well as their merging are
509 shown. The asterisk marks the cell used to create the graph shown on the right. **Right:** A
510 straight line (indicated in green color) was drawn from left to right onto the chosen image and
511 the pixel intensity along it plotted for both the Nup57-tDIMER and yEGFP-Tel1 images. The
512 vertical arrows indicate the points of maximal intensity, thus highlighting the proximity of
513 Tel1 signals to the nuclear periphery.
514

515 # Discussion

516 In this work, we have expanded the toolbox in the field of DSB sensing and repair.
517 First, we have taken advantage from the repetitiveness of the transposon elements in the
518 genome of *S. cerevisiae* to design gRNAs capable of driving Cas9 action at specific sites in the
519 genome. Upon Cas9 expression induction, we can compare otherwise identical genomes being
520 broken at an increasing number of locations by the same enzyme. We have validated
521 genetically, physically and functionally the performance of this system. Second, we used this
522 tool to characterize the behavior of the apical kinase of the DNA damage response Tel1. To
523 this end, we used a fluorescent tag at its N-terminus and checked that this did not alter its
524 main known functions in DNA damage sensing and telomere homeostasis. Next, we found
525 that Tel1 molecules congregate in the shape of foci in response to diverse sources of DSB.
526 Furthermore, we show for the first time that Tel1 can form up to 8 foci per cell, distributed in
527 the shape of a crown that seems to be in tight contact with the nuclear periphery.
528 Previous works have used the repetitiveness of the Ty elements in *S. cerevisiae* genome
529 to insert 2, 7 or 11 restriction sites that can be cut upon controlled induction of the HO
530 endonuclease (15,16). While the design behind our system is reminiscent of this one, we
531 managed to devise a wider range of induced cuts, thus permitting further studies on the dose-

532 dependency. Indeed, the Ty-HO system was used to assess, by Southern blot, the role of Mre11
533 on resection as well as, by monitoring the phosphorylation of the downstream effector Rad53,
534 the role of Tel1 in DNA damage signaling (15,16). Given the sensitivity of Southern and
535 western blotting, a maximum of 7 cuts was enough to assess functional differences. Yet, our
536 system provides an enlarged palette of induced DSBs suitable for less sensitive studies. A small
537 drawback of our system was its leakiness: without Cas9 induction, the basal level of Rad52
538 and of Rfa1 foci increased as a function of the gRNAs used to trigger 1, 15 or 59 cuts, so that
539 the basal number of cuts shown by the strain harboring the 59 DSBs vector doubles that shown
540 by cells without any gRNA (Fig 4B,C). Nevertheless, in spite of this significant basal difference,
541 the window of opportunity for inducing further breaks and characterize them was still wide
542 (Fig 4D,E and S2 Fig).

543 Tel1 binds DSBs irrespective of the cell cycle phase and, in agreement, Tel1 foci were
544 reported to form at any cell cycle stage, including G_1, in contrast with Rad52 foci, which are
545 mostly S- and G_2-restricted (30). Moreover, break binding by Tel1 occurs before repair is
546 undertaken either by NHEJ or by HR. In contrast, Rad52 binding is a marker of the
547 commitment of a break towards HR. Given these considerations, one would expect that the
548 percentage of cells in the population displaying Tel1 foci exceeds that of Rad52. Yet, the
549 kinetics, dose-dependency and percentages of both Rad52 and Tel1 foci formation were alike
550 when using the Cas9 system or in response to zeocin (compare Fig 4E with 5A and Fig 5B with
551 5C), suggesting a major commitment of breaks in both systems towards HR. In the case of
552 Cas9, the targeting of sequences sharing large homologies (Ty elements) may favor the use of
553 HR for repair. Moreover, the long residence time of the Cas9 nuclease on one side of the cut
554 after breaking (25) may obstruct NHEJ implementation. Similarly, bleomycins, a family to
555 which zeocin belongs, are also suggested to block DSBs ends (39). Thus, while both in human
556 and in *S. cerevisiae* cells NHEJ can achieve the repair of Cas9-induced breaks to different extents
557 (40–44), our confrontation of Tel1 *versus* Rad52 data suggests a major contribution of HR in the
558 face of these lesions in *S. cerevisiae.*

559 We exploited our system to compare the kinetics of damage sensing (Tel1), processing
560 (Rfa1, revealing resection) and HR engagement (Rad52). Upon Cas9 induction, cleavage
561 activity is persistent and, as fast as a break is repaired, it becomes available for cleavage again.
562 Further, Tel1 foci on a given DSB disappear when resection takes place (30). Thus, only the

563 curve slope speaks of the foci formation kinetics before the dynamic equilibrium is reached.
564 With this in mind, we first observed that the percentage of cells displaying Rfa1 foci is always
565 double that of cells displaying Tel1 or Rad52 foci, suggesting that resection progresses
566 comparatively for longer, thus increasing the residence time of Rfa1 bodies. We also observed
567 that the kinetics of foci formation of all three proteins are very similar for a given number of
568 cuts, indicating that the transition from one step to the next may take place very fast. Last, we
569 acknowledged a fair dose-dependent response in the number of such foci. An exception
570 concerns the x 15-cuts scenario, where Rfa1 foci formed in more cells, and Rad52 ones
571 appeared faster, than when 59 cuts were induced. This may highlight the phenomenon of
572 interference at clustered DSBs. Indeed, DSBs concentrated at near-by locations, as those
573 induced in the x 59-cuts scenario, are less efficiently repaired than isolated lesions (45).

574 More than 13 proteins working in the cascade of DSB sensing and repair have been
575 fluorescently labelled and their *in vivo* foci formation ability scored by microscopy (30,32,46).
576 With the exception of post-Spo11 cutting during meiosis, with up to 15 Rad52 foci measured
577 per cell (47), these proteins gather in a single focus irrespective of the number of DSBs. For
578 example, even at doses as high as 160 krad, which induces up to 80 DSBs per cell, haploid *S.*
579 *cerevisiae* cells as the ones used in this study eventually form a maximum of 2 Rad52 foci (47).
580 Of all this set, the only protein openly reported to simultaneously form multiple nuclear foci
581 is Rfa1, and these sites are identified as post-replicative repair territories (48). The difference
582 in whether the factor gathers under a single focus or as multiple foci may come from the nature
583 of the lesion to be repaired (a DSB *versus* a damaged but not broken template). Additionally,
584 the DNA-binding properties of the factor under consideration may restrict its mobility. For
585 example, Rfa1 remains bound to the DNA (49), perhaps preventing the nucleation of all breaks
586 at a single location. An interesting finding of our study is the evidence that Tel1 can form
587 multiple (up to 8) foci per cell in response to zeocin. So far, Tel1 is the only factor displaying
588 such a behavior when DSBs inducing agents are used in haploid *S. cerevisiae*. This ability could
589 relate to its role in sensing and not in processing. It may be that lesion recognition takes place
590 where it happened or, at the most, the gathering process during recognition is restricted to the
591 local environment. Later on, from the moment resection by nucleases takes place, the
592 processing and the subsequent steps are ruled by different nucleation abilities. In support of
593 these transitions, Tel1 foci were reported to colocalize neither with Rfa1 nor Rad52 ones (30),

594 and even subsequent downstream events, such as the processing of recombination
595 intermediates by nucleases like Slx4 or Mus81, do not occupy the same space as Rad52 centers
596 (32). This said, we noted that Tel1 formed only one focus in response to Cas9 nuclease
597 expression, irrespective of the dose of induced DSBs. This may relate to Ty retrotransposons,
598 which are targeted by Cas9 in our system, being clustered within a single nuclear subdomain
599 (50).

600 Analysis of numerous nuclei photographed from distinct angles led us to propose that
601 Tel1 foci form at the periphery of the nucleus, although not all over the sphere, but as a ring.
602 Additional proximity analysis visualizing a fluorescently tagged nucleoporin in order to
603 illuminate the nuclear periphery confirmed this notion. The fact that Tel1 foci form in close
604 contact to the nuclear periphery raises the prospect that a nucleation factor presumably exists
605 close to, or even at, the nuclear membrane that serves to scaffold them. Tel1 and the other
606 DNA damage response apical kinase, Mec1, are Phosphatidyl Inositol 3-kinase-like kinases.
607 Although these kinases are thought not to bear the ability to phosphorylate
608 phosphatidylinositol (PI) moieties any longer (51), they may have kept their ability to bind
609 such molecules. In agreement, the Mec1 human homolog, ATR, was reported to be assisted by
610 phosphoinositides in order to correctly nucleate in the shape of foci upon DNA damage (48).
611 Furthermore, ATR demonstrates ability to sense lipids at membranes (52), and to act at the
612 nuclear membrane to phosphorylate its targets in response to mechanical cues (53). Therefore,
613 it is very tempting to suggest that Tel1 is being guided at lipid hotspots at the inner nuclear
614 membrane either to exert its DNA breaks sensing activity, or to engage downstream actions
615 after having sensed them. In a further attempt to venture into this direction, we note the
616 striking similarity of the Tel1 foci-defined ring and the discrete spots described along the
617 nuclear-vacuole junction as marked by the Fatty Acids metabolism-related enzyme Mdm1
618 (54). It will be worth exploring in a near future whether Tel1 nucleation relates to the
619 metabolism of lipids.

620

621 **Acknowledgements**

622 We thank Philippe Pasero for strains, Olivier Gadal for the vector harboring *NUP57*-tDIMER, and Symeon
623 Siniossoglou for the vector permitting mCherry-Pus1 tagging. We acknowledge the imaging facility MRI, a member
624 of the national infrastructure France-BioImaging, supported by the French National Research Agency (ANR-10-
625 INBS-04, Investissements d'avenir). M.M.-C. thanks the ATIP-Avenir program, La Ligue contre le Cancer, la

Fondation ARC pour la Recherche sur le Cancer (COVID202001314) et l'Institut National du Cancer (PLBIO19-098 INCA_13832), France, for funding the research in her laboratory. B.P. thanks the Fondation ARC pour la Recherche sur le Cancer (ARCPJA22020060002119) for supporting his work.

Author Contributions: Conceptualization: B.P., M.M.-C.; **Data curation:** J.C., O.S., S.K., B.P., M.M.-C.; **Formal Analysis:** J.C., O.S., S.K., B.P., M.M.-C; **Funding acquisition:** B.P., M.M.-C.; **Investigation:** J.C., O.S., S.K., B.P., M.M.-C.; **Methodology:** S.K., B.P., M.M.-C.; **Project administration:** B.P., M.M.-C.; **Resources:** B.P.; M.M.-C.; **Supervision:** M.M.-C.; **Visualization:** B.P., M.M.-C; **Writing – original draft:** B.P., M.M.-C.; **Writing – review & editing:** J.C., O.S., S.K., B.P., M.M.-C.

Abbreviations:

CFP, Cyan Fluorescent Protein; **CPT**, camptothecin; **CRISPR**, Clustered Regularly Interspaced Short Palindromic Repeats; **DIC**, differential interference contrast; **DSBs**, Double Strand Breaks; **gRNA**, guide RiboNucleic Acid; **G_1**, Gap 1 phase; **G_2**, Gap 2 phase; **HR**, Homologous Recombination; **NHEJ**, Non-Homologous End Joining; **PAM**, protospacer adjacent motif; **PFGE**, pulsed field gel electrophoresis; **RFP**, red fluorescent protein; **S**, DNA synthesis phase; **WT**, wild type; **yEGFP**, yeast Enhanced Green Fluorescent Protein; **YFP**, Yellow Fluorescent Protein; **YNB**, yeast nitrogen base; **YEPD**, yeast extract peptone dextrose.

Competing Interests Statement

The authors declare no competing interests

References

1. Rouse J, Jackson SP. Interfaces between the detection, signaling, and repair of DNA damage. Science (80-). 2002;297(5581):547–51.
2. Pardo B, Gómez-González B, Aguilera A. DNA double-strand break repair: How to fix a broken relationship. Cell Mol Life Sci. 2009;66(6):1039–56.
3. Stein A, Kalifa L, Sia EA. Members of the RAD52 Epistasis Group Contribute to Mitochondrial Homologous Recombination and Double-Strand Break Repair in Saccharomyces cerevisiae. PLoS Genet. 2015;11(11):1–20.
4. Iacovoni JS, Caron P, Lassadi I, Nicolas E, Massip L, Trouche D, et al. High-resolution profiling of γh2AX around DNA double strand breaks in the mammalian genome. EMBO J. 2010;29(8):1446–57.
5. Peritore M, Reusswig K, Bantele SCS, Straub T, Peritore M, Reusswig K, et al. Strand-specific ChIP-seq at DNA breaks distinguishes ssDNA versus dsDNA binding and

660 refutes single-stranded nucleosomes Short Article Strand-specific ChIP-seq at DNA
661 breaks distinguishes ssDNA versus dsDNA binding and refutes single-stranded. Mol
662 Cell [Internet]. 2021;1–13. Available from: https://doi.org/10.1016/j.molcel.2021.02.005
663 6. Westmoreland JW, Summers JA, Holland CL, Resnick MA, Lewis LK. Blunt-ended
664 DNA double-strand breaks induced by endonucleases PvuII and EcoRV are poor
665 substrates for repair in Saccharomyces cerevisiae. DNA Repair (Amst) [Internet].
666 2010;9(6):617–26. Available from: http://dx.doi.org/10.1016/j.dnarep.2010.02.008
667 7. Lewis LK, Westmoreland JW, Resnick MA. Repair of endonuclease-induced double-
668 strand breaks in Saccharomyces cerevisiae: Essential role for genes associated with
669 nonhomologous end- joining. Genetics. 1999;152(4):1513–29.
670 8. Lewis LK, Kirchner JM, Resnick MA. Requirement for End-Joining and Checkpoint
671 Functions, but Not RAD52 -Mediated Recombination, after Eco RI Endonuclease
672 Cleavage of Saccharomyces cerevisiae DNA . Mol Cell Biol. 1998;18(4):1891–902.
673 9. Bellaiche Y, Mogila V, Perrimon N. I-SceI endonuclease, a new tool for studying DNA
674 double strand break repair mechanisms in Drosophila. Genetics. 1999;152(3):1037–44.
675 10. Rouet P, Smih F, Jasin M. Introduction of double-strand breaks into the genome of
676 mouse cells by expression of a rare-cutting endonuclease. Mol Cell Biol.
677 1994;14(12):8096–106.
678 11. Haber JE. A Life Investigating Pathways That Repair Broken Chromosomes. Annu
679 Rev Genet. 2016;50:1–28.
680 12. Plessis A, Perrin A, Habert JE, Dujon B. Site-specific Recombination Determined by I-
681 SceI, a Mitochondrial Group I Intron-Encoded Endonuclease Expressed in the Yeast
682 Nucleus. Genetics. 1992;130:451–60.
683 13. Choulika A, Perrin A, Dujon B, Nicolas JF. Induction of homologous recombination in
684 mammalian chromosomes by using the I-SceI system of Saccharomyces cerevisiae.
685 Mol Cell Biol. 1995;15(4):1968–73.
686 14. Gnügge R, Symington LS. Efficient DNA double-strand break formation at single or
687 multiple defined sites in the Saccharomyces cerevisiae genome. Nucleic Acids Res.
688 2020;48(20):1–10.
689 15. Llorente B, Symington LS. The Mre11 Nuclease Is Not Required for 5′ to 3′ Resection at
690 Multiple HO-Induced Double-Strand Breaks. Mol Cell Biol. 2004;24(21):9682–94.

691 16. Mantiero D, Clerici M, Lucchini G, Longhese MP. Dual role for Saccharomyces
692 cerevisiae Tel1 in the checkpoint response to double-strand breaks. EMBO Rep.
693 2007;8(4):380–7.
694 17. Wang R, Kamgoue A, Normand C, Léger-Silvestre I, Mangeat T, Gadal O. High
695 resolution microscopy reveals the nuclear shape of budding yeast during cell cycle
696 and in various biological states. J Cell Sci. 2016;129(24):4480–95.
697 18. Karanasios E, Barbosa AD, Sembongi H, Mari M, Han GS, Reggiori F, et al. Regulation
698 of lipid droplet and membrane biogenesis by the acidic tail of the phosphatidate
699 phosphatase Pah1p. Mol Biol Cell. 2013;
700 19. Tourrière H, Saksouk J, Lengronne A, Pasero P. Single-molecule Analysis of DNA
701 Replication Dynamics in Budding Yeast and Human Cells by DNA Combing. Bio-
702 Protocol. 2017;7(11):1–17.
703 20. Forstemann K, Hoss M, Lingner J. Telomerase-dependent repeat divergence at the 3'
704 ends of yeast telomeres. Nucleic Acids Res. 2000;28(14):2690–4.
705 21. Teixeira MT, Arneric M, Sperisen P, Lingner J. Telomere length homeostasis is
706 achieved via a switch between telomerase- extendible and -nonextendible states. Cell.
707 2004;117(3):323–35.
708 22. Mans R, Wijsman M, Daran-Lapujade P, Daran JM. A protocol for introduction of
709 multiple genetic modifications in Saccharomyces cerevisiae using CRISPR/Cas9. FEMS
710 Yeast Res. 2018;18(7):1–13.
711 23. Dicarlo JE, Norville JE, Mali P, Rios X, Aach J, Church GM. Genome engineering in
712 Saccharomyces cerevisiae using CRISPR-Cas systems. Nucleic Acids Res.
713 2013;41(7):4336–43.
714 24. Sheff MA, Thorn KS. Optimized cassettes for fluorescent protein tagging in
715 Saccharomyces cerevisiae. Yeast. 2004;21(8):661–70.
716 25. Sternberg SH, Redding S, Jinek M, Greene EC, Doudna JA. DNA interrogation by the
717 CRISPR RNA-guided endonuclease Cas9. Nature. 2014;507(7490):62–7.
718 26. Kim JM, Vanguri S, Boeke JD, Gabriel A, Voytas DF. Transposable elements and
719 genome organization: A comprehensive survey of retrotransposons revealed by the
720 complete Saccharomyces cerevisiae genome sequence. Genome Res. 1998;8(5):464–78.
721 27. Fleiss A, O'Donnell S, Fournier T, Lu W, Agier N, Delmas S, et al. Reshuffling yeast

722 chromosomes with CRISPR Cas9. PLoS Genet. 2019;15(8):1–26.
723 28. Matheson K, Parsons L, Gammie A. Whole-genome sequence and variant analysis of
724 W303, a widely-used strain of Saccharomyces cerevisiae. G3 Genes, Genomes, Genet.
725 2017;7(7):2219–26.
726 29. Weinert TA, Hartwell LH. The RAD9 gene controls the cell cycle response to DNA
727 damage in saccharomyces cerevisiae. Science (80-). 1988;241(4863):317–22.
728 30. Lisby M, Barlow JH, Burgess RC, Rothstein R. Choreography of the DNA damage
729 response: Spatiotemporal relationships among checkpoint and repair proteins. Cell.
730 2004;118(6):699–713.
731 31. Lisby M, Mortensen UH, Rothstein R. Colocalization of multiple DNA double-strand
732 breaks at a single Rad52 repair center. Nat Cell Biol. 2003;5(6):572–7.
733 32. Saugar I, Jiménez-Martín A, Tercero JA. Subnuclear Relocalization of Structure-
734 Specific Endonucleases in Response to DNA Damage. Cell Rep. 2017;20(7):1553–62.
735 33. Bernstein KA, Mimitou EP, Mihalevic MJ, Chen H, Sunjaveric I, Symington LS, et al.
736 Resection activity of the Sgs1 helicase alters the affinity of DNA ends for homologous
737 recombination proteins in Saccharomyces cerevisiae. Genetics. 2013;195(4):1241–51.
738 34. Menin L, Ursich S, Trovesi C, Zellweger R, Lopes M, Longhese MP, et al. Tel1/ ATM
739 prevents degradation of replication forks that reverse after topoisomerase poisoning .
740 EMBO Rep. 2018;19(7):1–13.
741 35. Nakada D, Matsumoto K, Sugimoto K. ATM-related Tel1 associates with double-
742 strand breaks through an Xrs2-dependent mechanism. Genes Dev. 2003;17(16):1957–
743 62.
744 36. Clerici M, Baldo V, Mantiero D, Lottersberger F, Lucchini G, Longhese MP. A
745 Tel1/MRX-Dependent Checkpoint Inhibits the Metaphase-to-Anaphase Transition
746 after UV Irradiation in the Absence of Mec1. Mol Cell Biol. 2004;24(23):10126–44.
747 37. Hirano Y, Fukunaga K, Sugimoto K. Rif1 and Rif2 Inhibit Localization of Tel1 to DNA
748 Ends. Mol Cell [Internet]. 2009;33(3):312–22. Available from:
749 http://dx.doi.org/10.1016/j.molcel.2008.12.027
750 38. Krol K, Brozda I, Skoneczny M, Bretne M, Skoneczna A. A genomic screen revealing
751 the importance of vesicular trafficking pathways in genome maintenance and
752 protection against genotoxic stress in diploid saccharomyces cerevisiae cells. PLoS

753 One. 2015;10(3):1–32.
754 39. Tam ATY, Pike BL, Hammet A, Heierhorst J. Telomere-related functions of yeast KU
755 in the repair of bleomycin-induced DNA damage. Biochem Biophys Res Commun.
756 2007;357(3):800–3.
757 40. Lemos BR, Kaplan AC, Bae JE, Ferrazzoli AE, Kuo J, Anand RP, et al. CRISPR/Cas9
758 cleavages in budding yeast reveal templated insertions and strand-specific
759 insertion/deletion profiles. Proc Natl Acad Sci U S A. 2018;115(9):E2010–47.
760 41. Román-Rodríguez FJ, Ugalde L, Álvarez L, Díez B, Ramírez MJ, Risueño C, et al.
761 NHEJ-Mediated Repair of CRISPR-Cas9-Induced DNA Breaks Efficiently Corrects
762 Mutations in HSPCs from Patients with Fanconi Anemia. Cell Stem Cell.
763 2019;25(5):607-621.e7.
764 42. van Overbeek M, Capurso D, Carter MM, Thompson MS, Frias E, Russ C, et al. DNA
765 Repair Profiling Reveals Nonrandom Outcomes at Cas9-Mediated Breaks. Mol Cell
766 [Internet]. 2016;63(4):633–46. Available from:
767 http://dx.doi.org/10.1016/j.molcel.2016.06.037
768 43. Tran NT, Bashir S, Li X, Rossius J, Chu VT, Rajewsky K, et al. With homologous
769 recombination factors. Front Genet. 2019;10(APR):1–13.
770 44. Jayavaradhan R, Pillis DM, Goodman M, Zhang F, Zhang Y, Andreassen PR, et al.
771 CRISPR-Cas9 fusion to dominant-negative 53BP1 enhances HDR and inhibits NHEJ
772 specifically at Cas9 target sites. Nat Commun [Internet]. 2019;10(1):1–13. Available
773 from: http://dx.doi.org/10.1038/s41467-019-10735-7
774 45. Nickoloff JA, Sharma N, Taylor L. Clustered DNA double-strand breaks: Biological
775 effects and relevance to cancer radiotherapy. Genes (Basel). 2020;11(1).
776 46. Chen H, Lisby M, Symington LS. RPA Coordinates DNA End Resection and Prevents
777 Formation of DNA Hairpins. Mol Cell [Internet]. 2013;50(4):589–600. Available from:
778 http://dx.doi.org/10.1016/j.molcel.2013.04.032
779 47. Lisby M, Rothstein R, Mortensen UH. Rad52 forms DNA repair and recombination
780 centers during S phase. Proc Natl Acad Sci U S A. 2001;98(15):8276–82.
781 48. Wong RP, García-Rodríguez N, Zilio N, Hanulová M, Ulrich HD. Processing of DNA
782 Polymerase-Blocking Lesions during Genome Replication Is Spatially and Temporally
783 Segregated from Replication Forks. Mol Cell. 2020;77(1):3-16.e4.

784 49. Miné-Hattab J, Heltberg M, Villemeur M, Guedj C, Mora T, Walczak AM, et al. Single
785 molecule microscopy reveals key physical features of repair foci in living cells. Elife.
786 2021;10:1–29.
787 50. O'Sullivan J. M., Sontam D. M., Grierson R. and Jones B. Repeated elements
788 coordinate the spatial organization of the yeast genome. Yeast. 2009;26:125–38.
789 51. Bradbury JM, Jackson SP. ATM and ATR. Curr Biol. 2003;13(12):468.
790 52. Zhang XH, Zhao C, Ma ZA. The increase of cell-membranous phosphatidylcholines
791 containing polyunsaturated fatty acid residues induces phosphorylation of p53
792 through activation of ATR. J Cell Sci. 2007;120(23):4134–43.
793 53. Kumar A, Mazzanti M, Mistrik M, Kosar M, Beznoussenko G V., Mironov AA, et al.
794 ATR mediates a checkpoint at the nuclear envelope in response to mechanical stress.
795 Cell. 2014;158(3):633–46.
796 54. Hariri H, Rogers S, Ugrankar R, Liu YL, Feathers JR, Henne WM. Lipid droplet
797 biogenesis is spatially coordinated at ER –vacuole contacts under nutritional stress .
798 EMBO Rep. 2018;19(1):57–72.
799

800

801 # Supporting Information

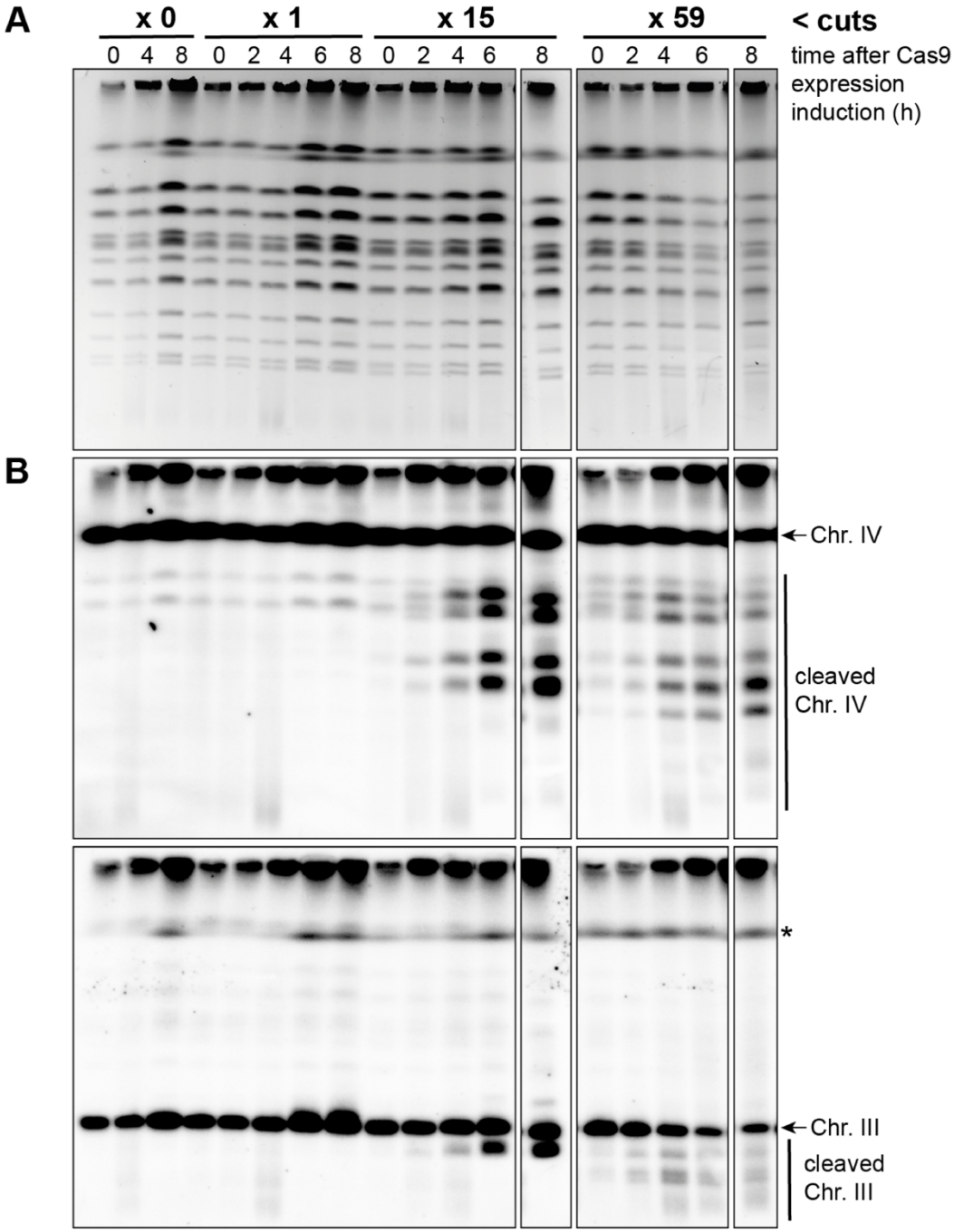

802

803 **S1 Fig. PFGE used for restriction analyses of chromosome cleavage by Cas9**

804 **A.** PFGE was prepared and run as in **Fig 2B**, and stained with ethidium bromide. Please note
805 that the time point 8 h for the x 15- and x 59-cuts were inadvertently exchanged during gel
806 loading. As such, the broken boxes indicate that the two lanes have now been replaced where
807 they belong.

808 **B.** Southern blot hybridizations against chromosome (Chr.) IV (top) and III (bottom) against
809 the DNA run in **(A)**. The asterisk denotes a residual band after incomplete stripping of
810 chromosome IV hybridization.
811

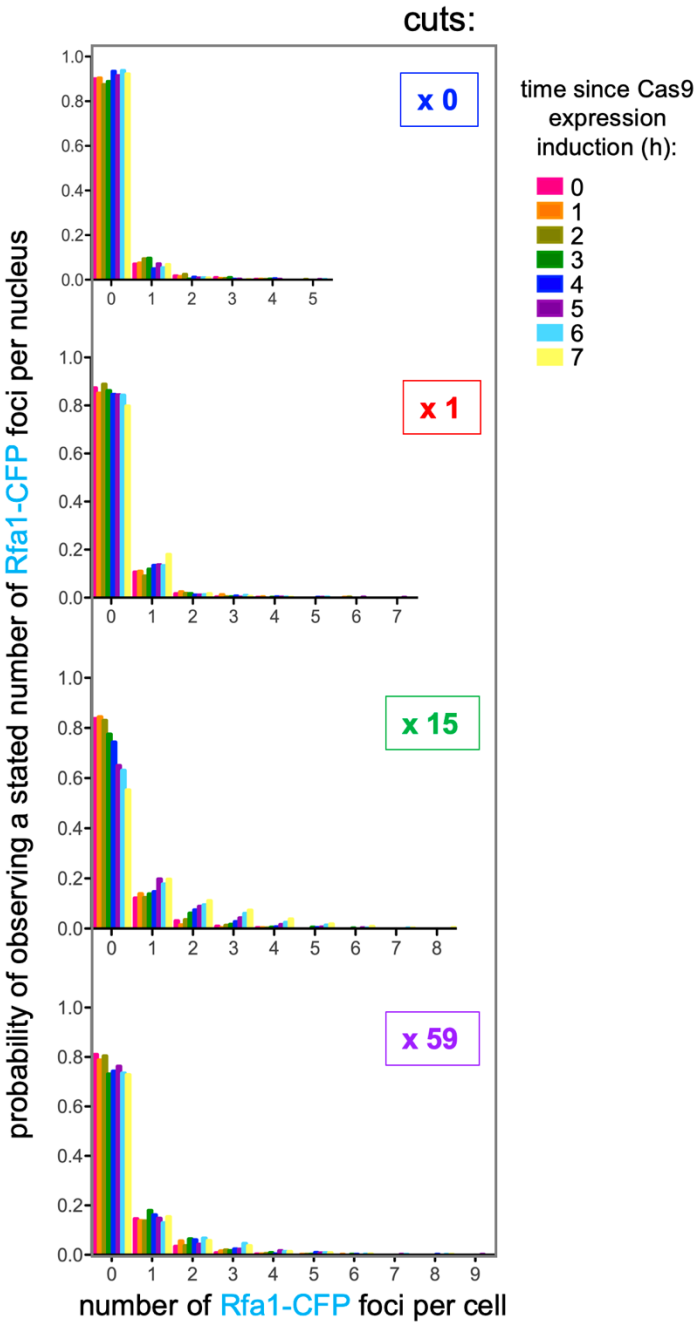

812
813 **S2 Fig. Quantification of the number of Rfa1-CFP foci per nucleus in response to Cas9 cuts**
814 Graphs showing the probability distribution of finding a stated number of Rfa1-CFP foci in a
815 given nucleus at a given time as calculated from the experiments presented in Fig 4D. The
816 probability distribution is calculated upon merging the three experiments presented in Fig 4D.

817 All three independent experiments had a similar profile. At least 200 cells were counted per
818 time-point, condition and experiment.
819
820

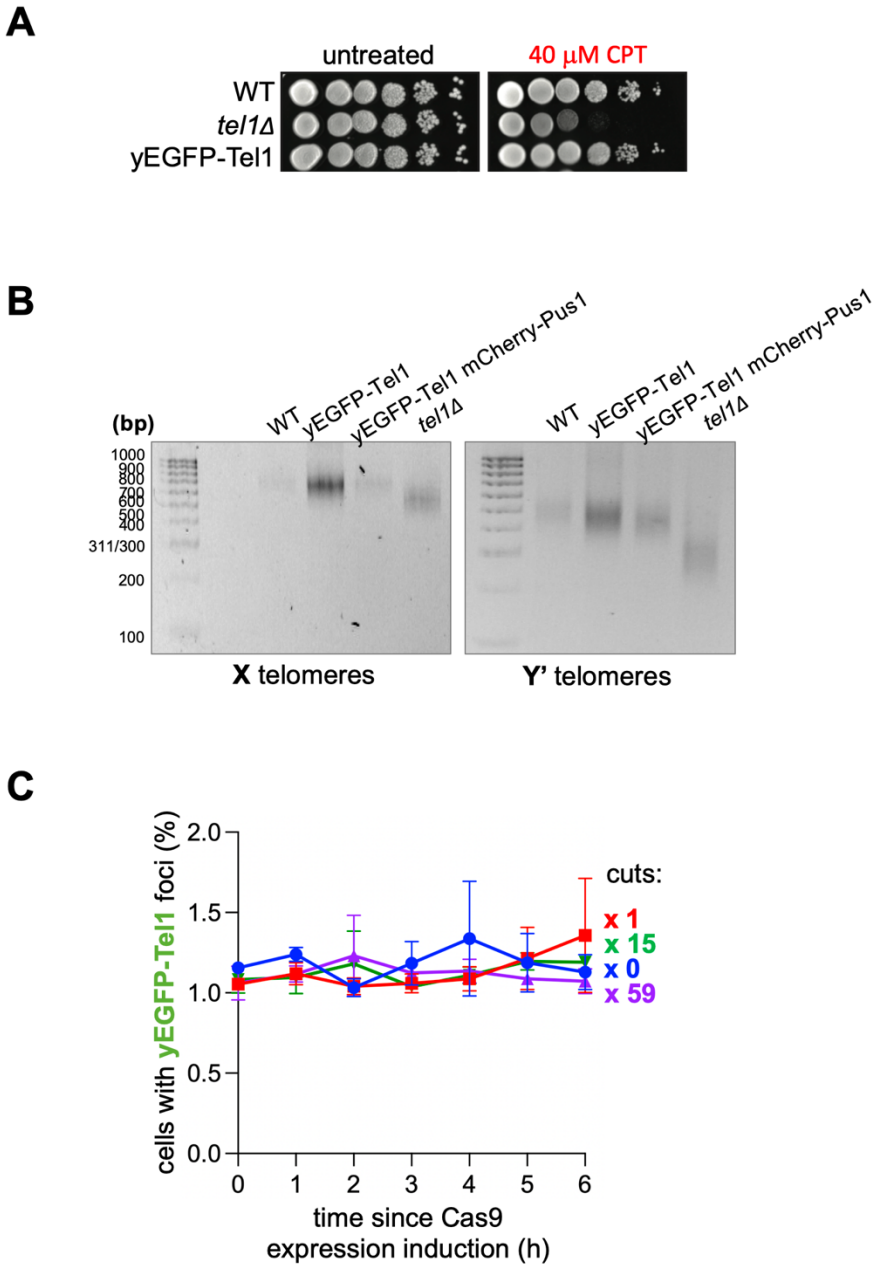

821
822 **S3 Fig. Controls ensuring that the yEGFP-Tel1-tagged strain behaves as a WT**
823 **A.** 10-fold serial dilutions of *S. cerevisiae* cells of the indicated genotypes spotted onto YPED
824 rich medium plates supplemented either with DMSO (untreated) or with 40 µM CPT,
825 incubated 2 to 3 days at 26°C and imaged.

826 **B.** Telomeres (X and Y′) length was measured by PCR-mediated amplification (see M&M) from
827 genomic DNA extracted from the indicated strains. *tel1Δ* cells were included as a control for
828 their telomere shortening phenotype. yEGFP-Tel1 cells, whether additionally bearing
829 mCherry-Pus1 or not, display WT-length telomeres.
830 **C.** The mean number of Tel1 foci per cell (as established by counting the total number of foci
831 divided by the total number of cells) was calculated out of at least 150 cells for each time point
832 and condition. This experiment was done three times, and the plotted value is the mean out of
833 those three experiments. The error bars correspond to the standard error of the mean associ-
834 ated to them.